

Spatiotemporal Characteristics of Snow Cover and Its Climate Impacts in the Western Tibetan Plateau Region

Ali Naqi¹, Chenghai Wang^{1*}, Xiang Feng¹, Sikandar Ali Junejo², Razzaq Ahmed³, Mohib Ullah¹

¹Key Laboratory of Arid Climate Resource and Environment of Gansu Province (ACRE), College of Atmospheric Sciences, Lanzhou University, Lanzhou, China

²Key Laboratory of Western China's Environmental Systems, College of Earth and Environmental Science, Lanzhou University, Lanzhou, China

³Department of Geography, Federal Urdu University of Arts Sciences and Technology, Karachi, Pakistan
Email: *wch@lzu.edu.cn

How to cite this paper: Naqi, A., Wang, C.H., Feng, X., Junejo, S.A., Ahmed, R. and Ullah, M. (2025) Spatiotemporal Characteristics of Snow Cover and Its Climate Impacts in the Western Tibetan Plateau Region. *Atmospheric and Climate Sciences*, 15, 549-577.

<https://doi.org/10.4236/acs.2025.153028>

Received: April 6, 2025

Accepted: May 23, 2025

Published: May 26, 2025

Copyright © 2025 by author(s) and Scientific Research Publishing Inc.

This work is licensed under the Creative Commons Attribution International License (CC BY 4.0).

<http://creativecommons.org/licenses/by/4.0/>



Open Access

Abstract

The western Tibetan Plateau (WTP; west of 80°E) represents a distinct geographical domain bounded by the Pamir Plateau, Karakoram Range, and Hindu Kush mountains. Characterized by perennial snow cover, this region plays a critical role in global and regional climate systems while serving as a vital freshwater reservoir for over 400 million people across the Indus, Amu Darya, and Tarim River basins. This study investigates spatiotemporal variations in snow cover fraction (SCF) and snow depth (SD) across the WTP from 1978 to 2020 using weekly snow cover data from the National Snow and Ice Data Center (NSIDC) and daily snow depth records from the National Tibet Plateau Data Center (TPDC). Results showed a significant decline in SCF at rates of -0.17% and $-0.93\% \text{ } 10 \text{ a}^{-1}$ during spring and summer, respectively, alongside a springtime reduction ($-0.02 \text{ cm } 10 \text{ a}^{-1}$) and slightly increase in summer ($0.001 \text{ cm } 10 \text{ a}^{-1}$) SD. These trends are attributed to rising seasonal temperatures (0.04°C and $0.02^\circ\text{C } 10 \text{ a}^{-1}$) and shifts in precipitation patterns (-0.16 mm and $+0.04 \text{ mm } 10 \text{ a}^{-1}$) in the same season. Correlation analyses identify that the ENSO IOBW, and TIOD show positive relationship with SCF reductions, while the NAO and SIOD show negative correlation. These findings underscore the sensitivity of WTP snow cover to climatic drivers and water resource management for downstream regions in South and East Asia.

Keywords

Snow Cover Fraction (SCF), Snow Depth (SD), Western Tibetan Plateau (WTP), Seasonal Variability, General Circulation, Sea Surface Temperature (SST)

1. Introduction

Snow cover constitutes a critical component of the Earth's climate system, influencing regional and global climate dynamics through surface albedo modulation, energy balance adjustments, and hydrological cycle regulation [1] [2]. The Tibetan Plateau (TP) hosts the most extensive snow cover in the mid-low latitudes of the Northern Hemisphere, with particularly abundant snow accumulation and high snow cover fraction (SCF) in the western Tibetan Plateau (WTP), which encompasses the Pamir Plateau and portions of the Karakoram and Kunlun mountain ranges, where average elevations exceed 4000 meters [3]. Snow cover in the WTP is not only vital for maintaining regional water security across Central, Western and Southern Asia through meltwater contributions but also plays a pivotal role in regulating regional and global climate by altering surface radiation and thermal energy balance [4] [5].

Climate projections show significant seasonal and spatial shifts in precipitation across the TP, with CMIP6 high-emission scenarios (e.g., SSP5-8.5) suggesting increased precipitation and associated glacier and flood risks, particularly in the Pamirs and southeastern regions [6]. Warming-driven reductions in tundra zones up to 70% in Asia under a 2°C scenario pose serious implications for snow cover and water resources [7]. High-resolution regional modeling indicates the WTP may experience extreme warming (>10°C under SSP5-8.5) alongside stronger monsoonal and westerly influences [8]. Long-term observations also reveal declining snow cover and depth, especially in the Pamirs and western TP, largely due to elevation-dependent warming and earlier melt onset [9] [10].

Over the past few decades, global warming has driven a marked decline in WTP snow cover, raising concerns about water resource sustainability, ecosystem stability, and climate feedback mechanisms [11]-[13]. The glacier extent in the upper Beas basin is projected to decline by up to 100% by the end of the 21st century, leading to a significant reduction in glacier-sourced runoff. Despite this loss, total streamflow may slightly increase due to rising temperatures and precipitation [14]. For example, the Himalayas exhibit consistent snow cover reduction [15]-[19], whereas WTP's subregions like the Karakoram range demonstrate increasing trends of snow cover, which are known as the "Karakoram Anomaly" [20] [21]. Notably, WTP snow formation is closely linked to westerly airflows transporting moisture from Europe and Central Asia, contrasting with the Indian monsoon-dominated moisture supply in the plateau's central-eastern sectors [22] [23].

The WTP's snow cover also exhibits substantial interannual variability in extent and duration, primarily driven by fluctuations in regional temperature and precipitation [4] [24]. For instance, [25] reported divergent snow cover patterns across the TP from 1979 to 2018, with overall stable snow depth (SD) and snow cover days (SCD) but notable decreases in the Nyainqentanglha Mountains (WTP subregion) and increases in the Kunlun Mountains. Recent analyses (2000-2021) indicate that 23.0% of the TP experienced SCD reductions (predominantly south-

eastern TP), while 4.9% (mainly northwestern TP) showed increase [26]. Given that snow cover change over the WTP lacks a consistent trend, understanding this interannual variability is crucial for accurately forecasting water availability and assessing potential impacts on downstream regions dependent on WTP meltwater.

The interplay between snow cover characteristics and key climate variables like temperature and precipitation in the WTP is complex. Interannual snow cover fluctuations demonstrate strong negative correlation with *in-situ* temperatures, particularly in February, April, May, August, and September [24]. Additionally, TP snow cover fraction exhibits a significant negative correlation with precipitation [8]. Climate oscillations such as the North Atlantic Oscillation (NAO) and El Niño-Southern Oscillation (ENSO) further modulate snowpack dynamics by influencing the South Asian summer monsoon and mid-latitude circulation, though mechanistic linkages remain unclear [27]-[30]. Similarly, the tropical Western/Eastern Indian Ocean precipitation dipole exerts poorly quantified influences on cold-season snowfall, particularly in December [31] [32]. Despite these insights, a critical knowledge gap persists regarding the relative contributions of climatic drivers to WTP snow cover variability, particularly the interplay between temperature, precipitation, and large-scale climate modes (e.g., ENSO, NAO).

This study employs a multi-faceted analytical framework integrating remote sensing, climate reanalysis, and statistical methods to address three research questions: 1) How has climate warming impacted snow cover on the WTP? 2) Which climatic systems predominantly control snow cover changes on the WTP? 3) How do snow cover changes influence water resources in downstream regions? The paper is structured as follows: Section 2 outlines the data and methodology; Section 3 discusses the spatiotemporal characteristics of snow cover; Section 4 highlights the snow cover variability and mechanism; and Section 5 concludes the study with a discussion of the findings and their implications.

2. Data Methods

2.1. Study Area

The study area located between latitudes 30°N and 40°N, and longitudes 60°E and 80°E (Figure 1), is a high-altitude region that forms part of the TP, the highest and largest plateau on Earth [33]. This area is characterized by its rugged and complex topography, including vast desert plains, mountainous regions, and glaciers, with elevations frequently exceeding 4,000 meters which is critical for regional hydrology and climate, influencing major river systems and monsoonal patterns [34]. The WTP (study area), bordered by the Pamir Plateau, Karakoram Range, and Hindu Kush, features rugged terrain with elevations reaching 8240 m.

Climatically, the WTP is influenced by the intersection of the Indian Monsoon in the south and the westerlies in the north, leading to significant spatial variability in precipitation patterns. The WTP, as a key region within the TP, plays a pivotal

role in influencing local and remote atmospheric circulations, making it an essential area for studying land-atmosphere interactions and climate change impacts [13]. Summers are relatively mild compared to other high-altitude regions, with average temperatures ranging from 10°C to 15°C , whereas winters are harsh, with temperatures often dropping below -20°C [35]. Snow cover in the region is seasonal, typically occurring between September and April, with snow depth and duration varying in response to changing climatic conditions [36].

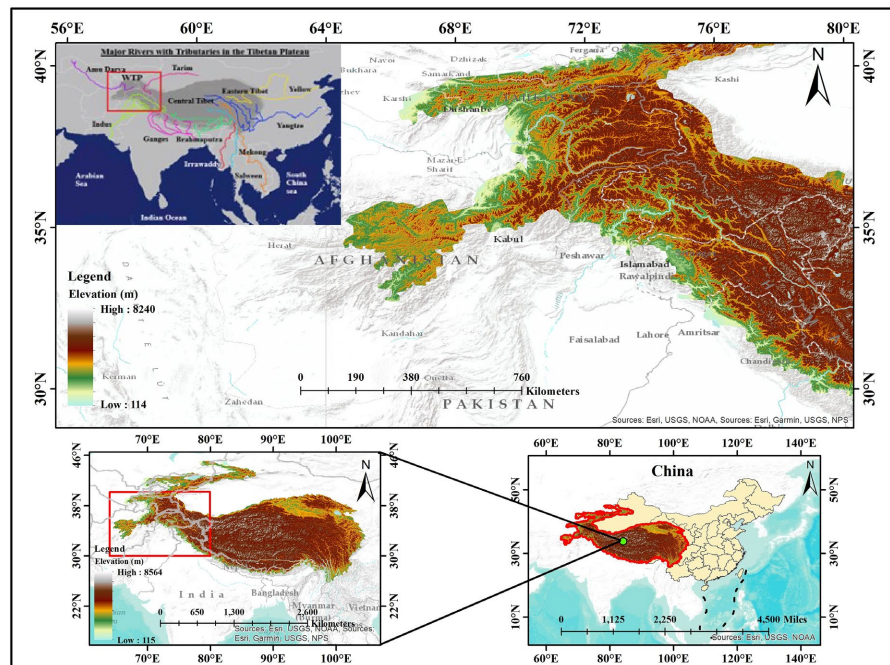


Figure 1. Map showing the WTP region, highlighting its elevation gradient (114 m to 8240 m). The inset map provides the broader context of the study area within TP and the top-left figure shows the major river basins of the WTP.

The WTP has importance for the water supply of millions of people across India, Pakistan, and China, highlighting the region's importance for both regional ecosystems and human populations [35]. As climate change affects the cryosphere, the glaciers and snow cover of the TP are undergoing noticeable changes, which could significantly impact water resources in the downstream regions [33]. TP is also a key area for monitoring climate change, as it is particularly sensitive to shifts in temperature and precipitation, which can accelerate glacial retreat and alter water availability [36]. Studies of snow cover, glacier mass balance, and hydrological processes in this region are essential for understanding the broader implications of climate change on the Asian monsoon system and water availability for millions of people [35].

2.2. Data

This study utilizes multiple datasets to provide a comprehensive analysis of snow cover and associated climatic variables over an extended period, with the aim of

understanding long-term trends and their driving factors. The National Snow and Ice Data Center's (NSIDC) "Northern Hemisphere EASE-Grid 2.0 weekly snow cover and sea ice extent" dataset [37], provides a comprehensive record of sea ice and snow cover dynamics from 3 October 1966 to 1 January 2023, ensuring consistency and long-term climate analysis. With a 7-day temporal resolution and a 25 km × 25 km spatial resolution (Table 1), the data are derived from multiple satellite platforms and sensors, mapped using the NSIDC EASE-Grid 2.0 projection (EPSG:6931) for seamless geospatial integration. This dataset is invaluable for assessing changes in snow cover and ice dynamics, particularly in the context of evolving climate conditions. It offers insights into the evolution of key cryosphere components within the spatial framework of the EASE-Grid 2.0 projection, balancing both regional detail and hemispheric coverage.

Table 1. Description of remote sensing and reanalysis datasets utilized in this study.

No.	Product name	Spatial Resolution	Temporal resolution	Time Span	Variables	References
1	NSIDC EASE-Grid 2.0 Ver.4	25 km × 25 km	Weekly	1978-2023	SCF	[37]
2	TPDC a	25 km × 25 km	Daily	1979-2021	SD	[38]
3	ERA5	10 km × 10 km	Monthly	1950 to 2024	T., Pre., W b, GPH c, Q d	[39]
4	NCC e	25 km × 25 km	Monthly	1951-2023	Climate Index	[40]

^aNational Tibetan Plateau Data Center/Third Pole Environment Data Center, ^bU and V wind components, ^cGeopotential Height, ^dSpecific Humidity, ^eNational Climate Center of China.

Remote sensing data plays a crucial role in analyzing long-term climate trends and their impact on snow cover variability. The daily snow depth dataset from 1979 to 2019, derived from National Tibet Plateau Data Center's (TPDC) using SMMR, SSM/I, and AMSR-E passive microwave remote sensing dataset with a resolution of 0.25° × 0.25°, was utilized [38] [41]. Monthly snow depth dataset on 1° × 1° grids were averaged from the daily dataset. With 43 years of continuous observations, this dataset enables robust analysis of spatiotemporal snow cover dynamics. The extended time period allows for a thorough examination of snow cover variability, providing important insights into how climate change is affecting snow-dominated regions. This has significant implications for water resources, hydrology, and regional climate patterns across the Northern Hemisphere.

To explore the relationship between general circulation patterns and snow cover, the ERA5 monthly reanalysis data from the European Centre for Medium-Range Weather Forecasts (ECMWF) was employed. ERA5 offers a continuous high-resolution record of atmospheric variables from 1940 to present, making it essential for understanding the interaction between snow cover and atmospheric processes. Monthly snow cover data at a 24-kilometer resolution, combined with variables such as temperature, sea surface temperature (SST), and precipitation [39], facilitate a comprehensive analysis of the climatic drivers influencing snow cover. To

examine the relationship between snow cover and climate indices El Niño-Southern Oscillation (ENSO), Indian Ocean SST (IOSST), and North Atlantic Oscillation (NAO) supplementary independent variable datasets were acquired from China's National Climate Centre (NCC) [40].

2.3. Methods

2.3.1. Non-Parametric Trend Detection (Mann-Kendall Test)

The non-parametric Mann-Kendall test was used to assess temporal trends in snow cover, temperature, and precipitation over the WTP. The test evaluates a statistic, “ S ”, for data series that are stationary and independent, represented as X_t (where $t = 1, 2, 3, \dots, n$, and n denotes the length of the series). The Mann-Kendall statistics is computed as follows:

$$S = \sum_{i=1}^{n-1} \sum_{j=k+1}^n \text{sign}(X_j - X_i) \quad (1)$$

where X is the time series variable, and positive and negative values of S indicate upward and downward trends, respectively. The statistical significance of the detected trends was evaluated using the associated p -values, with trends considered statistically significant at the 95% confidence level ($p < 0.05$). This test was applied to both annual and seasonal data.

2.3.2. Simple Linear Regression

To assess snow cover variation and understand regional snow trends, simple linear regression was employed. This method provides a robust framework for analyzing both temporal and spatial variations in snow cover over the WTP. Regions with statistically significant trends ($p < 0.05$) are highlighted by hatching on the corresponding maps.

2.3.3. Multivariate Correlation (Pearson's r)

The Pearson correlation coefficient (r) was used to quantify the relationship between snow cover and various meteorological factors, including precipitation, temperature, general circulation patterns, and climate indices. For each observation n , let x_j and y_j represent the values of snow cover and the corresponding meteorological element, respectively. The average values of these variables are denoted by \bar{x}_j and \bar{y}_j . The correlation coefficient r is calculated as:

$$r = \frac{\sum (x_i - \bar{x}_j)(y_i - \bar{y}_j)}{\sqrt{\sum (x_i - \bar{x}_j)^2 \sum (y_i - \bar{y}_j)^2}} \quad (2)$$

where r ranges from -1 to 1 , and n is the number of observations. A positive r ($r > 0$) indicates a positive correlation, while a negative r ($r < 0$) suggests a negative correlation. The statistical significance of the correlation was tested using Student's t -test.

2.3.4. Root Mean Square Error (RMSE)

Root Mean Square Error (RMSE) was used to assess the strength of relationships

between snow cover and climatic factors. RMSE is especially useful for evaluating the performance of regression models by quantifying the deviation between observed and predicted values. The formula for RMSE is:

$$\text{RMSE} = \sqrt{\frac{1}{n} \sum_{i=1}^n (y_i - \hat{y}_i)^2} \quad (3)$$

where y_i is the observed value for the i^{th} data point, \hat{y}_i is the predicted value for the i^{th} data point, and n is the total number of observations. RMSE was calculated for snow cover in relation to temperature (T) and precipitation (Pre.) for four seasons defined as follows: winter (December-January-February, DJF), spring (March-April-May, MAM), summer (June-July-August, JJA), and autumn (September-October-November, SON) as well as annually.

3. Spatiotemporal Characteristics of Snow Cover over WTP

3.1. Spatial Patterns of Snow Cover

To examine the spatial variation in snow cover over the WTP, we analyzed its distribution, which is largely influenced by topography and climatic conditions. **Figure 2(a)** displayed the annual mean and standard deviation (std.) of snow cover across the region. The largest snow cover fraction (SCF) is observed in the northern and higher-altitude areas, particularly between 36°N and 44°N latitude. These areas consistently exhibit SCF values above 48%, with some regions reaching up to 80% (**Table 2**). The darker red areas indicate regions of significant snow accumulation, driven by colder temperatures and higher precipitation rates in these elevated zones. Seasonal or temporal variability in SCF is evident, with northern regions maintaining high snow cover, while certain areas show reduced snow cover, reflecting seasonal thawing patterns. This variability underscores the dynamic nature of snow cover, which changes depending on the season and specific climatic conditions during the study period.

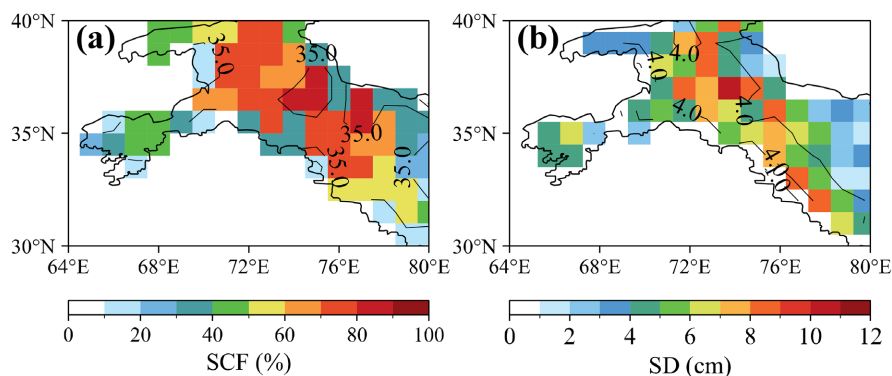


Figure 2. (a) Mean (shading) and std. (black contours: %) of SCF for annual. (b) is same as (a) but for SD (std.; black contours: cm). The blue dashed line represents the study region.

The largest SD is concentrated in the northern and higher-altitude regions (**Fig-**

ure 2(b)), consistent with the SCF distribution. SD in these areas often exceeds 8 cm, with some locations recording depths greater than 12 cm. The spatial distribution of SD demonstrates a clear north-south gradient, with deeper snow accumulations in the northern part of the plateau. This gradient is influenced by the orographic effect, where higher elevations receive more snowfall. These findings highlight the dynamic nature of snow cover, which necessitates continuous monitoring to assess the impacts of climate change on snow dynamics. Understanding these patterns is essential for effective water resource management, as snowmelt from these regions contributes significantly to river flows and water availability downstream. The results emphasize the need for integrated climate and hydrological models to predict future changes and develop adaptive strategies in response to ongoing climate shifts.

Four distinct seasons DJF, MAM, JJA, and SON were focused on interannual variability of seasonal snow cover. By analyzing the mean SCF and its std. for each season, we aimed to better understand the spatial and temporal patterns of snow cover dynamics. During the winter, snow cover reached its highest levels, with extensive and consistent coverage in the northern and higher-altitude areas (Figure 3(a)). The mean SCF often exceeded 80%, reflecting a strong snowpack maintained by frequent snowfall (Table 2). The low std. observed during this season indicates a high degree of inter-annual consistency in winter snow cover.

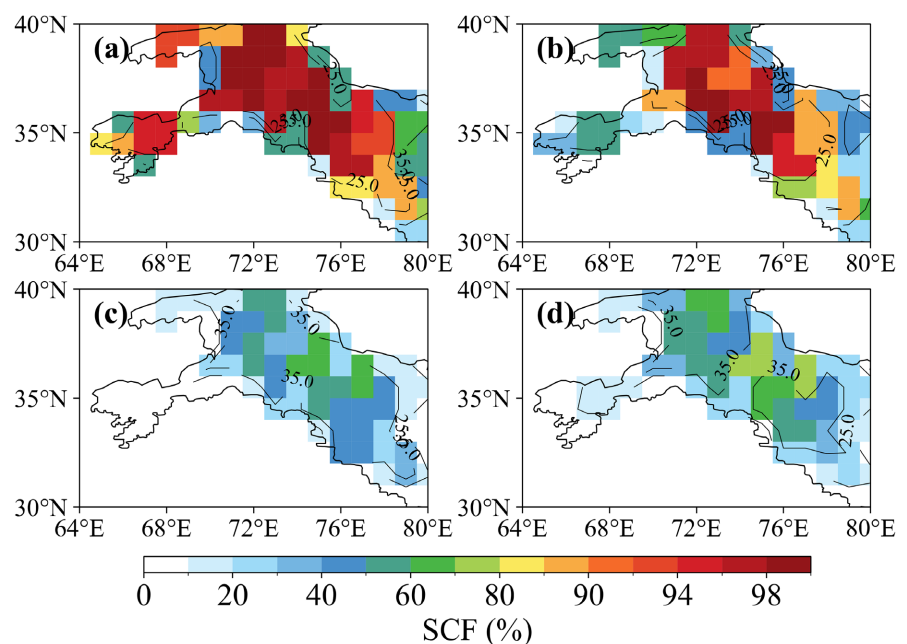


Figure 3. Seasonal mean SCF (%) for (a) DJF, (b) MAM, (c) JJA, and (d) SON, with corresponding std. (black contours: %) for the period of 1972-2022. The blue dashed rectangle indicates the study region.

As temperatures rose in spring, snow cover began to melt significantly, especially in the southern and lower-elevation regions (Figure 3(b)). This transition

period saw a marked decrease in SCF, accompanied by higher std. values, indicating increased variability in snow cover. The variability was primarily driven by the interaction between the residual winter snowpack and spring thawing, which varied depending on specific climatic conditions, such as temperature anomalies and precipitation patterns during the spring months. In summer, snow cover reached its lowest point, with the mean SCF dropping below 20% in most areas, and only the highest elevations retaining some snow (**Figure 3(c)**). This season exhibited the highest std., reflecting substantial inter-annual variability. The extent of summer snow cover was highly sensitive to prevailing summer temperatures and precipitation, leading to considerable differences in snow cover from one year to the next. The minimum snow cover in summer highlighted the importance of climatic conditions during this season in determining snow persistence at high altitudes.

Autumn marked the beginning of snow accumulation again, especially in the northern and higher-altitude areas. The mean SCF gradually increased as temperatures dropped and early snowfall occurred (**Figure 3(d)**). However, the std. remained moderate, reflecting variability in the timing and extent of these early snowfalls. The differences observed in autumn snow cover was influenced by the timing of early winter weather patterns and the onset of significant snowfall events. This transitional phase is critical for understanding the buildup of the winter snowpack, which plays a key role in the hydrological cycle and regional climate dynamics.

The average SCF during the DJF displayed a clear concentration of snow cover in the northern and higher-altitude regions (**Figure 3(a)**). The darker shades, indicating higher SCF values, were primarily located between 36°N and 44°N, with the highest concentration observed in the northwestern areas. This distribution pattern suggests a strong influence of both altitude and latitude on SCF, as higher elevations and northern latitudes experience colder temperatures that are conducive to snow accumulation. Moving southward and to lower altitudes, SCF progressively decreased, highlighting the spatial variability of snow cover due to topographic and climatic differences.

Table 2. Seasonal and annual matrices of average SCF (%) and SD (cm) from 1978 to 2020 over the WTP.

Season	SCF (%)				SD (cm)			
	Mean	Std.	Max	Min	Mean	Std.	Max	Min
DJF	76.51	20.55	100	0.00	7.64	3.65	38.07	0.00
MAM	63.23	26.50	100	0.00	6.21	2.97	32.53	0.00
JJA	27.61	30.01	100	0.00	1.81	1.71	34.76	-0.10
SON	34.19	31.07	100	0.00	1.89	1.75	27.69	0.00
Annual	50.39	36.78	84.42	7.53	4.39	3.95	19.33	0.03

Table 3. Seasonal and annual matrices of average Pre. (mm/day) and T_{avg} ($^{\circ}$ C) from 1978 to 2020 over the WTP.

Season	Pre. (mm/day)				T_{avg} ($^{\circ}$ C)			
	Mean	Std.	Max	Min	Mean	Std.	Max	Min
DJF	41.78	9.45	252.90	0.00	-3.47	8.59	10.54	-19.93
MAM	53.22	7.65	260.10	0.00	-14.12	2.29	18.72	-35.36
JJA	32.20	20.45	502.70	0.00	-4.15	4.38	31.53	-28.29
SON	21.31	12.68	481.50	0.00	7.29	1.65	33.02	-16.74
Annual	37.13	32.99	502.70	0.00	-2.90	5.92	27.37	-31.24

The std. of SCF during winter also revealed notable seasonal variability (**Figure 3(a)**). While the northern regions continued to exhibit high SCF, certain areas showed a significant reduction in snow cover, reflecting the effects of seasonal melting and natural fluctuations. This variation underscores the dynamic nature of snow cover in response to seasonal temperature changes. The highest seasonal variability was observed in the eastern part of the WTP, suggesting these areas are more susceptible to seasonal shifts, potentially due to their specific climatic conditions or elevation profiles. These findings emphasize the importance of topography and climate in shaping the distribution and variability of snow cover over the plateau, reinforcing the need for continuous monitoring to understand the impacts of climate change.

The distribution of SD exhibited a clear gradient from north to south, with the deepest snow accumulations observed in the northern, higher-altitude regions (**Figure 4(c)**), which was consistent with the SCF distribution. The central and southern parts of the region showed shallow snow depths, indicating that these areas received less snowfall or experienced faster snowmelt due to seasonal transitions from spring to summer. This pattern of SD variation aligned with the region's topography, where mountainous areas with higher elevations naturally accumulate more snow. Understanding SD is critical for evaluating snowpack water storage, which directly impacts water resource management in the region.

The SD distribution highlighted in **Figure 4(d)** further emphasized the changes in snow accumulation and melting cycles. The northern regions continued to exhibit substantial SD, although reductions were observed compared to the mean SD distribution (**Figure 4(c)**), indicating the influence of seasonal melting. In contrast, the southern regions showed minimal changes in SD, reflecting their limited snow accumulation capacity. The eastern regions, however, displayed more significant seasonal variations, likely influenced by specific climatic factors or localized weather patterns.

During winter, SD peaked, particularly in the northern and higher-altitude areas (**Figure 4(a)**), with mean values often exceeding 16 cm. This substantial accumulation was driven by frequent and heavy snowfall. The low std. observed in winter indicated a high degree of consistency in SD across years, reflecting stable

and predictable winter snowfall patterns. This consistency is essential for snowpack water storage, which plays a key role in maintaining river flows during the drier months. As spring progresses and temperatures rise, SD exhibited a marked decrease (**Figure 4(b)**). The mean SD showed a dramatic decline compared to winter, particularly in lower-altitude and southern regions. The increase in std. during MAM indicated greater variability in SD, likely due to fluctuations in temperature, wind patterns, geopotential heights (GPH), and precipitation. The spring season marked a critical transitional period when snow accumulation and melt rates impacted water availability and hydrological cycles.

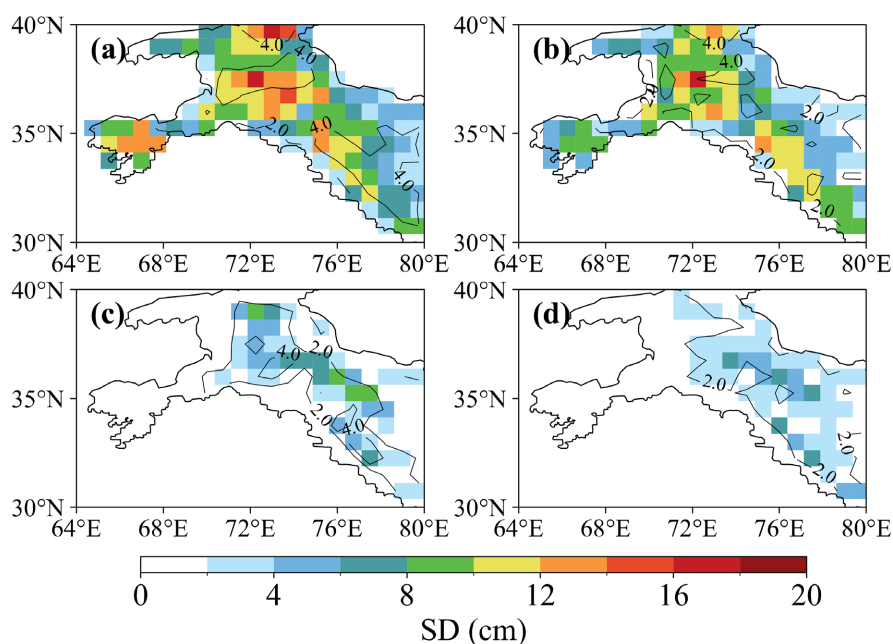


Figure 4. Seasonal mean SD (cm) for (a) DJF, (b) MAM, (c) JJA, and (d) SON, with corresponding std. (black contours: cm) for the period of 1972-2022. The blue dashed rectangle indicates the study region.

In summer, the mean SD reached its lowest values, reflecting extensive melting across the region (**Figure 4(c)**). Most areas saw SD values below 5 cm, with only the highest altitudes retaining some snow. The high std. during summer highlighted significant inter-annual variability in SD, driven by fluctuations in summer temperatures and precipitation (**Table 3**). The minimal SD in summer underscored the sensitivity of snowpack to climatic conditions during this period. In autumn, SD began to rise as temperatures dropped and early snowfall events occurred (**Figure 4(d)**). The mean SD increased, particularly in the northern and higher-altitude regions, signaling the start of the snow accumulation period. The moderate std. in autumn reflected some variability in the timing and extent of early snowfalls. This season served as a preparatory phase for the build-up of the winter snowpack, with the timing of initial snow accumulation playing a key role in shaping SD patterns for the upcoming winter.

3.2. Temporal Changes Characteristics of Snow Cover

Figure 5 illustrates the annual anomalies in SCF and SD over the region (35°N - 40°N , 70°E - 75°E) from 1978 to 2020. The SCF anomaly exhibits a modest annual mean increase of 0.64%, while SD shows a slightly higher anomaly of 0.73 cm (**Table 4**). The proximity of these values suggests interannual variability in snow-pack dynamics, with SD anomalies displaying marginally greater sensitivity to climatic drivers. The black dashed lines representing std imply moderate interannual fluctuations, though the SCF anomaly's lower magnitude underscores potential regional-scale buffering against extreme annual snow cover changes.

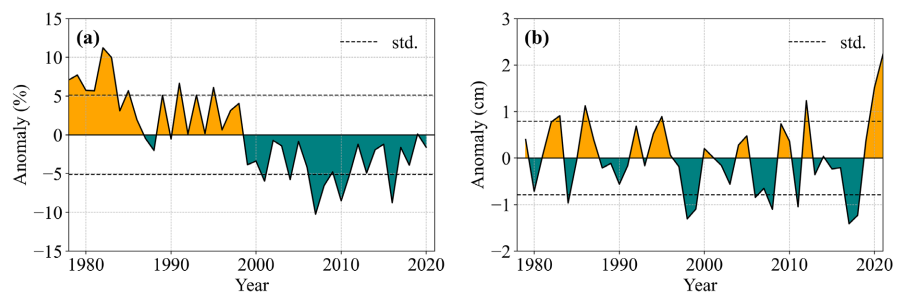
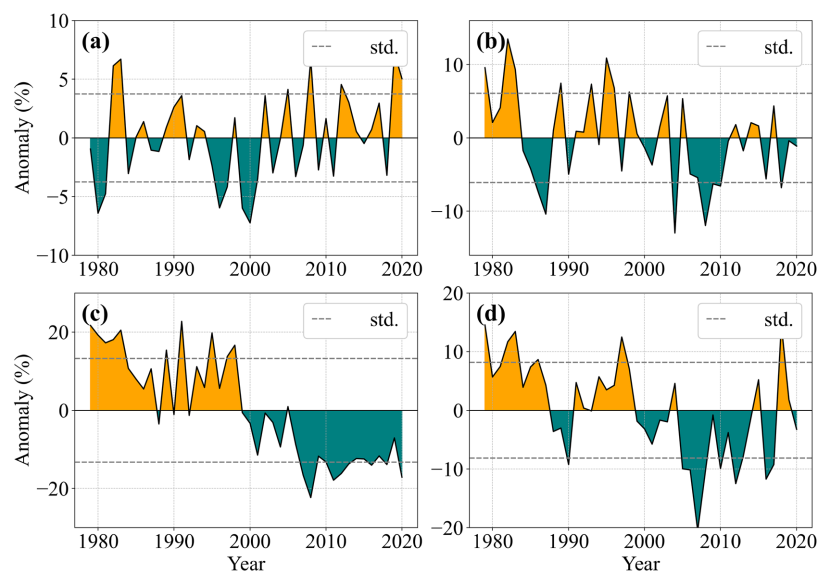


Figure 5. (a) Annual anomalies (1978-2020) in regional SCF (%) and (b) is same as (a) but for SD (cm) over 35°N - 40°N , 70°E - 75°E . Dashed lines denote ± 1 standard deviation (std.).

Seasonal SCF anomalies (**Figures 6(a)-(d)**, **Table 4**) reveal pronounced heterogeneity. The largest anomaly occurs in JJA (13.24%), contrasting with the DJF (3.76%) and MAM (6.10%) values. This elevated summer anomaly likely reflects prolonged snow retention in high-elevation zones of the Hindu Kush and western Himalayas, where seasonal temperature gradients and topographic influences delay melt processes. SON (8.15%) anomalies further suggest earlier snowfall onset, potentially linked to shifting atmospheric circulation patterns. The stark seasonal differences highlight the region's sensitivity to intra-annual climatic shifts.



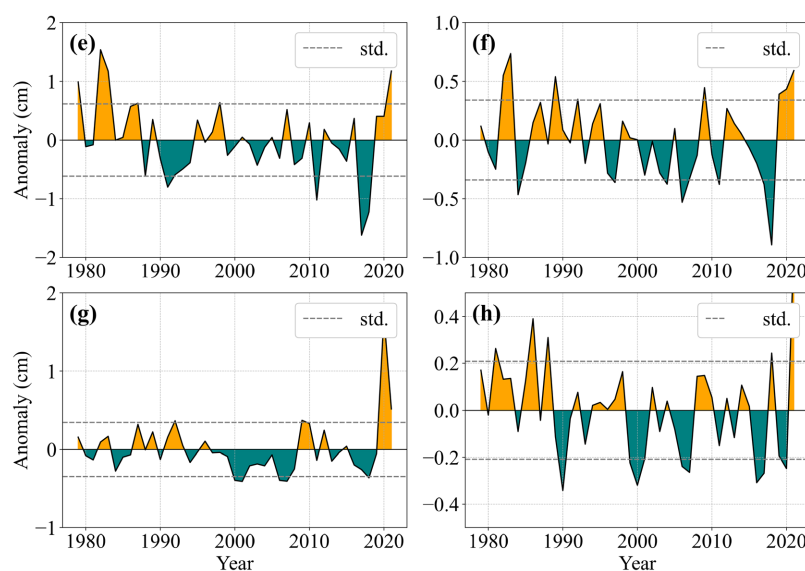


Figure 6. Seasonal anomalies in SCF (%) and SD (cm) from 1979 to 2020 over the region (35°N - 40°N , 70°E - 75°E). (a)-(d) SCF anomalies for DJF, MAM, JJA, and SON, respectively. Positive (yellow) and negative (green) bars indicate above and below average snow cover, respectively, with black dashed lines representing the std. (Figures 7(e)-(h)) the same as in (Figures 7(a)-(d)) but for snow depth (SD) anomalies.

SD anomalies (Figures 6(e)-(h)) exhibit distinct seasonality, peaking in DJF (1.26 cm) and diminishing to a minimum in SON (0.40 cm). Winter's higher SD anomaly aligns with enhanced snowfall accumulation under colder temperatures, while the lower SON anomaly may reflect transitional snowpack instability during autumn freeze-thaw cycles. Notably, MAM SD anomalies (0.67 cm) are subdued compared to SCF (6.10%), implying spring snowmelt reduces SD despite persistent spatial coverage—a critical factor for regional hydrology.

The decoupling of SCF and SD anomalies in certain seasons (e.g., MAM) suggests differing climatic controls. Spring's high SCF anomaly (6.10%) paired with low SD (0.67 cm) points to widespread but shallow snowpack, likely due to intermittent snowfall and rapid melt. Conversely, DJF's moderate SCF (3.76%) but higher SD (1.26 cm) anomalies indicate localized, deeper accumulations, possibly from intense snowfall events. Such disparities underscore the need to disentangle spatial extent from snow mass in climate impact assessments.

The study region spans WTP high-altitude zones, where complex topography amplifies microclimatic variability. The elevated summer SCF anomaly (13.24%) may arise from orographic precipitation and glacial feedbacks, which sustain summer snow cover in shadowed valleys or north-facing slopes. Conversely, lower annual anomalies (SCF: 0.64%, SD: 0.73 cm) suggest compensating seasonal trends for instance, increased summer retention offsetting reduced winter accumulation highlighting the region's role as a climatic transition zone.

The black dashed std. lines in Figure 5 and Figure 6 denote considerable inter-annual variability, particularly in JJA SCF and DJF SD. Extreme anomalies implied by wider std. bands could correlate with erratic monsoon moisture incur-

sions or Arctic oscillation phases. Such variability poses challenges for water resource management, as snowpack serves as a freshwater reservoir for downstream basins. The annual SD anomaly's consistency (0.73 cm) further signals a gradual shift in snow mass, with implications for groundwater recharge.

The observed anomalies have profound hydrological consequences. Enhanced JJA SCF may delay meltwater release, altering river discharge timing and affecting agriculture in arid lowlands. Conversely, reduced SON SD anomalies (0.40 cm) could advance melt onset, exacerbating water scarcity in pre-monsoon months. These trends align with broader climate projections for High Mountain Asia, where warming temperatures perturb snow-rain transitions. Continuous monitoring is critical to refine regional climate models and inform adaptive strategies. The interplay of seasonal SCF and SD anomalies underscores the region's climatic complexity, driven by topography, atmospheric dynamics, and warming trends.

Table 4. Seasonal and annual regional std. and anomalies (1978-2020) of SCF (%) and SD (cm) over 35°N-40°N, 70°E-75°E. Std. Values represent deviations from the long-term mean.

Seasons	SCF (%)		SD (cm)	
	Std.	Anomaly	Std.	Anomaly
DJF	3.76	1.20×10^{-14}	1.26	-1.78×10^{-15}
MAM	6.10	1.42×10^{-14}	0.67	4.02×10^{-16}
JJA	13.24	-8.12×10^{-15}	0.75	4.97×10^{-16}
SON	8.15	3.30×10^{-15}	0.40	1.22×10^{-16}
Annual	6.51	-6.94×10^{-15}	0.64	-1.76×10^{-16}

The annual and seasonal trends in snow cover across the WTP (30°N-40°N, 62°E-80°E) exhibited substantial spatial and temporal variations, offering valuable insights into the evolving dynamics of the regional cryosphere (Figure 7). On an annual scale (Figure 7(a) & Figure 7(b)), a pronounced and statistically significant decline in SCF has been observed, with reductions surpassing 5% in multiple regions, particularly in the central and southern parts of the study domain. This decline in SCF is mirrored by a corresponding decreased in SD, with reductions exceeding 0.5 cm in several locations. These negative trends in both SCF and SD suggest that increasing temperatures are playing a pivotal role in destabilizing snowpack accumulation and persistence. While most areas exhibited decreasing trends, some isolated regions in the northern and northeastern parts of the WTP demonstrated slight positive trends in SD, which may be attributed to localized increases in winter precipitation or shifting atmospheric moisture transport mechanisms.

Moreover, the annual SCF is decreasing steeply with a rate of -0.416 % per decade ($p < 0.01$). In contrast, temperature showed a significant positive increase with slope 0.025 °C per decade. As well as the annual averages showed highly signifi-

cant correlations for both SCF and SD (-0.58), confirming that temperature is the dominant factor driving snow cover changes in the study region. A critical examination of temporal trends (**Figure 7(c)**) revealed a statistically significant decline in SCF and SD, further corroborating the overarching trend of snow cover reduction over the study period. The concurrent increase in temperature over the same period, with a positive trend exceeding 0.025°C per decade, reinforces the hypothesis that rising temperatures are the primary driver of these snowpack reductions. Interestingly, precipitation trends did not exhibit statistical significance, indicating that variations in snowfall accumulation were less influential than temperature-driven snowmelt processes in determining overall snow cover trends. These findings aligned with broader global and regional climate trends, wherein increasing temperatures exerted a dominant influence on cryospheric dynamics.

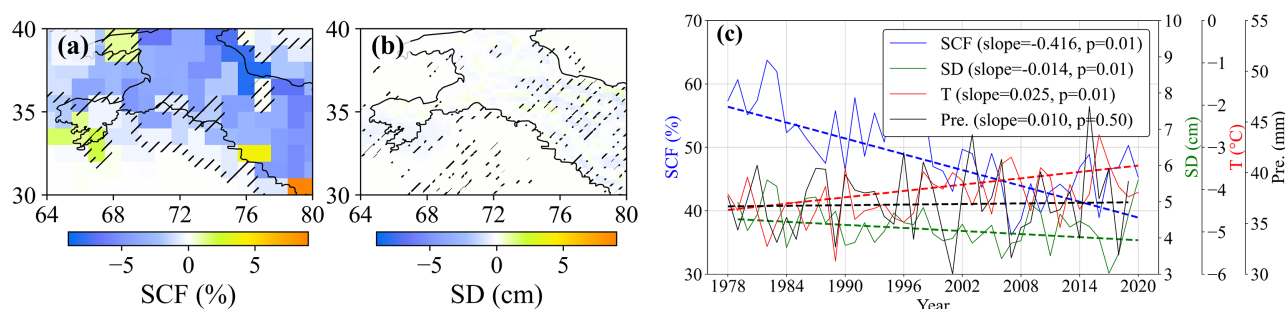


Figure 7. (a) & (b) spatial distribution of annual trends for SCF (%), SD (cm). The black hatchings show 95 % confidence level. (c) temporal trends for SCF, SD, T ($^{\circ}\text{C}$), and Pre. (mm) over the study period. P values show the significance level.

Seasonal analyses of SCF and SD trends (**Figures 8(a)-(h)**) highlighted intricate seasonal variations shaped by complex climatic and topographic interactions. In winter (**Figure 8(a)**), widespread negative trends dominated the western and southern regions, with SCF reductions exceeding 10% in some areas. These patterns are consistent with rising winter temperatures, which likely contribute to reduced snow accumulation and increased melting during the season. Similarly, SD trends in winter showed pronounced decreases (**Figure 8(e)**), particularly in mid-altitude regions that are highly sensitive to temperature fluctuations. However, some localized areas in the northeastern domain exhibited slight positive trends in SD, potentially due to enhanced winter precipitation WTP. Furthermore, a strong negative correlation ($r = -0.70$) was observed in the DJF season, suggesting that rising temperatures (1978-2020) contributed significantly to the decrease in SCF.

Spring emerged as the season with the most extensive reductions in both SCF and SD. Even high-altitude regions, which typically maintain snow cover longer duration, experienced notable declines (**Figure 8(b)** & **Figure 8(f)**). This suggested an accelerated onset of snowmelt, likely driven by rising spring temperatures. The implications of these trends were particularly significant for hydrology, as snowmelt-driven water availability plays a crucial role in sustaining downstream water resources for agriculture, hydropower, and ecosystem health. More-

over, a weaker negative correlation of -0.52 was observed, which is still notable, although not as strong as in winter (Table 5). For SD, correlations were less significant in the MAM and JJA seasons (Table 5), with weak correlations. However, RMSE values remained significant for these periods, indicating that temperature had a moderate but important influence on SD in these seasons.

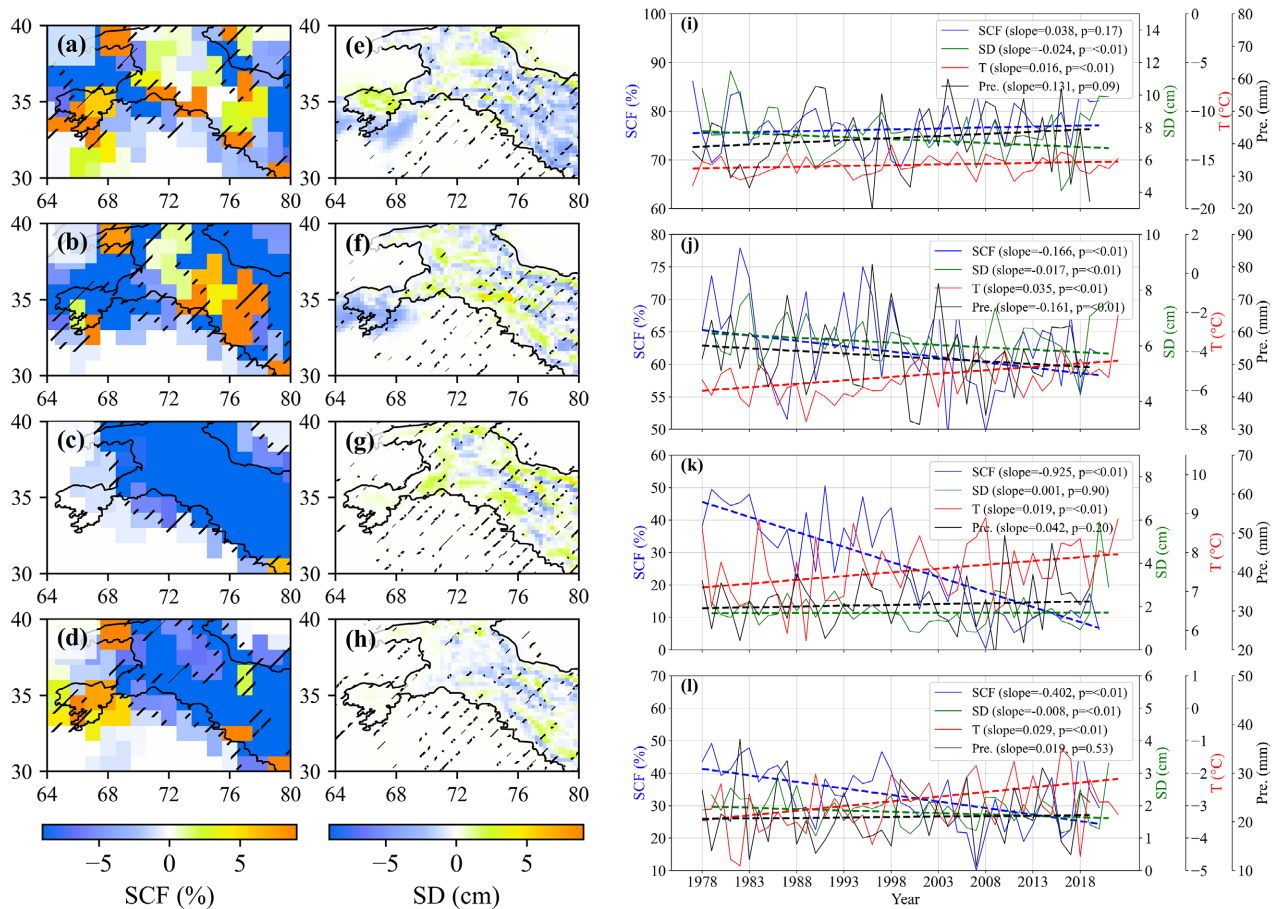


Figure 8. Panels (a) to (d) show the spatial distribution trends for SCF during the DJF, MAM, JJA, and SON. Panels (e) to (h) are the same but for SD respectively. Black hatchings show 95 % confidence level. Panels (i) to (l) depict the temporal trends for SCF, SD, T, and Pre., with p -values indicating the significance level.

Table 5. Results of linear regression analyses for SCF (%) and SD (cm), Average monthly T (T_{avg} ; °C), and Pre. (mm/day) from 1978 to 2020 across all seasons.

Season	SCF (%/10a)	SD (cm/10a)	Tavg (°C/10a)	Pre. (mm/10a)
DJF	0.038	-0.024**	0.016**	0.131*
MAM	-0.166**	-0.017**	0.035**	-0.161**
JJA	-0.925**	0.001	0.019**	0.042
SON	-0.402**	-0.008**	0.029**	0.019
Annual	-0.416**	-0.014**	0.025**	0.01

** : Significant at $p < 0.05$, marginally significant ($0.05 \leq p \leq 0.1$)*.

Summer trends showed minimal snow cover across much of the region, except at the highest elevations where perennial snow persists (**Figure 8(c)** & **Figure 8(g)**). Within these high-altitude zones, SD trends exhibited mixed signals, with some areas experiencing slight increases and others showing reductions. This suggested a dynamic balance between reduced summer snowfall and delayed snowmelt, potentially influenced by shifting atmospheric circulation patterns. The sensitivity of high-altitude snow cover to summer warming underscored the importance of monitoring these regions for long-term cryospheric stability.

Autumn represented a transitional period, with SCF and SD trends reflecting the combined influences of delayed early-season snowfall and residual warming effects from summer (**Figure 8(d)** & **Figure 8(h)**). Negative SCF trends are particularly prominent in the central and southern regions, suggesting delayed snow accumulation and potential reductions in early-season snowfall. These trends aligned with observed increases in autumn temperatures, which can inhibit early snow formation and reduce overall seasonal snow storage. Additionally, a strong negative correlation (-0.67) demonstrated in this season, further supporting the hypothesis that warming temperatures are contributing to a decrease in SCF (**Table 5**). However, the correlation for SD in the SON season was weaker (-0.26), and the RMSE for SCF was less significant compared to SD, indicating that temperature has a more pronounced influence on SD in autumn than on SCF.

The temporal trends of SCF, SD, temperature, and precipitation across four seasons (**Figures 8(i)-(l)**) further substantiated the overarching patterns observed in the spatial analyses. In all seasons, SCF exhibits a clear and statistically significant negative trend, reinforcing the consistent long-term decline in snow cover. The SD trends followed a similar trajectory, albeit with some seasonal variations in magnitude. Temperature trends remain significantly positive across all seasons, highlighting the pervasive influence of warming on snow dynamics. Conversely, precipitation trends displayed more variability, with some seasons exhibiting slight increases or decreases, but none reaching statistical significance. This indicated that while precipitation variability influences inter-annual snow cover fluctuations, the dominant control on long-term snowpack reductions is temperature-driven ablation.

These results have profound implications for water resources, ecosystem stability, and regional climate interactions. The decline in snow cover, particularly during spring and autumn, highlighted the increasing vulnerability of the cryosphere to climate change. Spring snowmelt is a critical contributor to river discharge and water availability in many parts of the region, and its acceleration could disrupt hydrological cycles and water resource management. Similarly, delayed snow accumulation in autumn could lead to longer periods of bare ground, influencing soil moisture levels, vegetation growth, and surface energy balance.

Moreover, the annual and seasonal variability of these trends underscored the need for a more nuanced understanding of the atmospheric processes and feedback mechanisms driving snow cover changes. Topographic factors, such as ele-

vation, aspect, and slope, play a crucial role in modulating snow retention and melt rates. Future research should focus on integrating high-resolution climate models with remote sensing and *in-situ* observations to better capture these complexities and improve predictions of future snow cover changes.

Table 6. Pearson's Correlation Coefficient (r) between snow cover matrices (SCF and SD) and climate factors (T and Pre.) across seasonal and annual scales (1978-2020).

Season	Pearson's " r "			
	T _{avg} & SCF	T _{avg} & SD	Pre. & SCF	Pre. & SD
DJF	-0.70	-0.61	0.41	0.31
MAM	-0.52*	-0.32*	-0.15	-0.01
JJA	-0.52*	-0.24*	0.06	-0.15
SON	-0.67*	-0.26*	0.23	-0.14
Annual	-0.73*	-0.58*	0.13	0.26

** : Significant at $p < 0.05$, Marginally significant ($0.05 \leq p \leq 0.1$)*.

The results provided compelling evidence of a persistent and significant decline in snow cover across WTP from 1978 to 2020. The consistency of these trends underscored the urgent need to address the impacts of climate change on the snow cover. As warming continues to accelerate, the implications for hydrology, agriculture, and regional climate dynamics will become increasingly pronounced. Developing effective adaptation and mitigation strategies will be essential for managing the long-term consequences of these changes, particularly in regions that rely on water resources. Continued monitoring and research are imperative to enhance our understanding of the intricate interactions between climate, snow cover, and regional environmental systems. In conclusion, while precipitation plays a secondary role in influencing snow cover, temperature remains the primary driver of changes in both SCF and SD. These findings highlight the critical impact of rising temperatures on the cryosphere, particularly in regions where snow is a vital water resource.

4. Climate-snow cover linkages in the WTP: Variability and Mechanisms

4.1. The Relationship between Climate and Snow Cover

The correlation between SCF and climate indices over the WTP region during the autumn reveals how large-scale oceanic and atmospheric phenomena influence snow conditions (Figure 9). Each sub-plot presented the correlation between SCF and a specific climate index, offering insights into their regional impacts. The ENSO showed a positive (negative) correlation with SCF, particularly in the eastern and southwestern parts of WTP. Higher Niño3 values were associated with reduced SCF during the autumn months. Similarly, the Niño1+2 index displayed

a strong positive correlation with SCF in the western and central regions, with statistically significant results ($p < 0.05$), highlighting the influence of the Niño1+2 pattern on SCF in these areas (Figure 9).

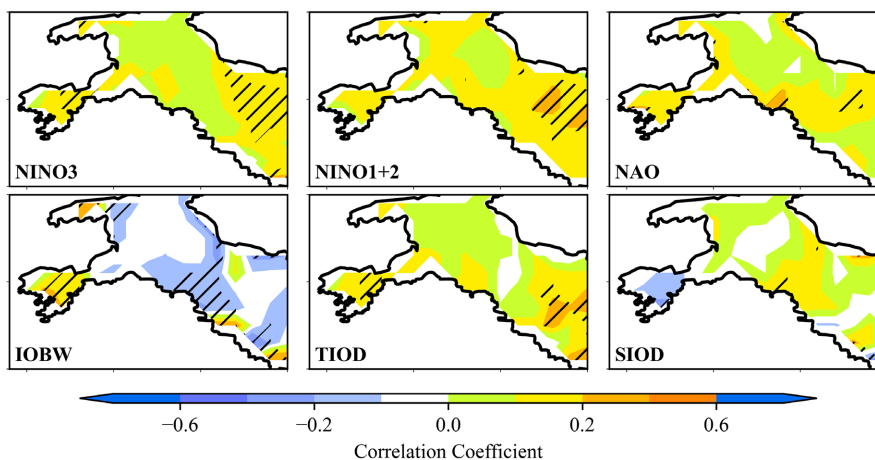


Figure 9. Spatial correlation patterns between SCF (%) and climate: Niño3, Niño1+2, NAO, IOBW, TIOD, and SIOD. Areas with dashed lines show a 99 % confidence level.

The North Atlantic Oscillation (NAO) showed a positive correlation with SCF in the northeastern and central regions, suggesting that a stronger NAO is linked to increased snow cover in WTP (Figure 9). Conversely, the Indian Ocean Basin-Wide (IOBW) pattern exhibited a insignificant negative (positive) correlation where $r = 0.029$ with SCF (Table 6), indicating a complex interaction between IOBW and snow cover dynamics in the WTP region (Figure 9). Further analysis revealed that the Tropical Indian Ocean Dipole (TIOD) exhibited a mixed pattern, with both positive and negative correlations in the eastern and western parts of WTP, indicating that minor TIOD variations, often linked to sea surface temperature conditions, have a modest impact on SCF (Figure 9). Similarly, the Southern Indian Ocean Dipole (SIOD) demonstrated a positive correlation with SCF in the central and southeastern parts of the WTP, suggesting that changes in SIOD conditions are associated with variations in snow cover in these regions (Figure 9).

The SCF was significantly influenced by multiple climate indices. The Niño3 and Niño1+2 patterns showed strong positive correlations in the eastern, southwestern, and central regions, with higher Niño3 values linked to reduced SCF. The NAO, was strongly positively correlated with SCF in the central and northeastern regions, indicating that increased NAO activity led to enhanced SCF. The IOBW, TIOD, and SIOD, showed region-specific correlations. Notably, TIOD and SIOD had a modest impact on SCF in the eastern and southeastern regions. Collectively, these patterns highlighted the complex and significant role that large-scale climate indices play in shaping autumn SCF variation in the WTP. The climate patterns, Niño3, Niño1+2, NAO, IOBW, TIOD, and SIOD, have distinct but often region-specific influences on snow cover in the WTP. These patterns interact in complex ways, reflecting the sensitivity of snow cover to large-scale climatic conditions.

Correlations between SD and climate indices revealed large-scale climatic drivers of autumn SD variability across the WTP (**Figure 10, Table 7**). The Niño3 index exhibited a positive correlation ($r = 0.201$) with SD (**Figure 10, Table 7**), particularly in central and eastern regions, where reduced Niño3 values corresponded to heightened SD. This relationship likely stems from intensified westerly moisture advection toward the plateau during negative Niño3 phases. The Niño1+2 index demonstrated stronger regional coherence, with a robust correlation ($r = 0.251$) in western areas and moderate associations centrally, implicating Tibetan High activation in SD suppression through subsidence-driven drying. Spatial heterogeneity characterized the NAO index, with positive correlations in northern WTP contrasting with negative linkages in western sectors (**Figure 10**). Enhanced NAO phases appear to amplify jet stream-driven moisture variability, redistributing precipitation northward and diminishing SD in arid western zones. As previously noted, the IOBW index's weak negative correlation ($r = -0.054$) with SST patterns reflects dynamically complex mid-latitude interactions, potentially via anticyclonic suppression over the WTP that restricts moisture convergence. The TIOD correlated positively with SD in the eastern WTP (**Figure 10**), where positive TIOD phases enhance cross-equatorial Somali jet moisture transport, elevating snowfall. Similarly, the SIOD displayed positive correlations in central regions, aligning with Mascarene High-modulated storm track shifts that amplify SD variability through orographic uplift. These teleconnections highlight region-specific mechanisms: Niño1+2 and TIOD govern western and eastern moisture pathways, respectively, while SIOD and NAO modulate synoptic-scale storm activity. The IOBW's subdued signal suggests its influence is secondary to localized atmospheric blocking. Collectively, these linkages underscore the mechanistic role of climate indices in governing autumn SD dynamics. Negative Niño3 and positive TIOD/SIOD phases enhance moisture influx, whereas Tibetan High intensification and NAO-driven jet stream variability suppress SD regionally. Such patterns emphasize the WTP's sensitivity to both tropical and extratropical forcing, with implications for hydrological forecasting in a warming climate.

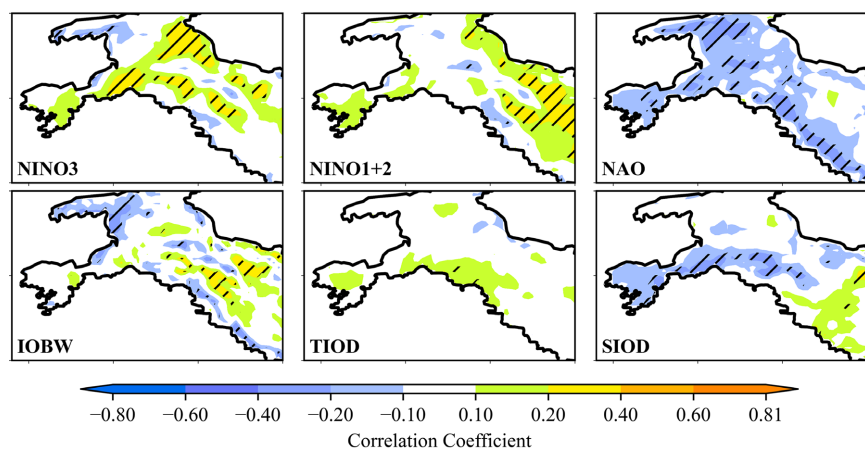


Figure 10. Spatial correlation patterns between SD (cm) and climate: Niño3, Niño1+2, NAO, IOBW, TIOD, and SIOD. Areas with dashed lines show a 99 % confidence level.

Table 7. Pearson Correlation Coefficient (r) between snow cover, and climate during SON (Autumn) season.

Indices	Grid cells * (%)		Pearson's " r "	
	SCF	SD	SCF	SD
Niño3	4.23	9.12	0.049	0.201
Niño1+2	11.27	11.16	0.114	0.251
NAO	1.41	0.93	-0.181	-0.148
IOBW	22.54	3.72	0.029	-0.054
TIOD	2.82	6.79	0.241	0.204

*: Percentage of statistically significant grid cells ($p = 0.05$ level) relative to the total study area; '-' indicates negative correlation.

The correlation analysis between SCF and climate indices during autumn over the WTP reveals significant region-specific influences of large-scale climate patterns (Figure 9, Table 7). The ENSO, particularly the Niño3 and Niño1+2 indices, showed varying impacts on SCF, with Niño3 linked to reduced SCF in the eastern and southwestern regions, and Niño1+2 correlated positively with SCF in the western and central regions. The NAO had a positive correlation with SCF in the northeastern and central areas, while the IOBW index showed complex, often insignificant, effects on snow cover. The TIOD and SIOD indices displayed mixed correlations, with TIOD influencing the eastern and western parts and SIOD affecting the central and southeastern regions. For SD, Niño3 showed a positive correlation in the central and eastern regions, while the Niño1+2 index exhibited strong correlations in the western region. The NAO showed mixed correlations, with a positive link in the north and a negative one in the west. These findings emphasize the significant, yet complex, roles that climate indices play in shaping snow cover variations across the WTP during autumn.

4.2. Possible Mechanisms Linked to Snow Cover Variation

The seasonal analysis of atmospheric circulation and moisture flux anomalies (Figure 11) reveals a dynamically interconnected framework of large-scale processes that govern regional hydroclimatic variability, with profound implications for snow cover dynamics. During winter (Figure 11(a)), the pronounced negative water vapor flux anomalies over Central Asia (CA) and the TP reflect robust moisture divergence, driven by intensified northerly wind vectors that channel cold, dry air masses from Siberia. Concurrently, positive flux anomalies over the Arabian Sea and Indian subcontinent signify moisture convergence, sustained by the advection of humid air from the tropics. Crucially, the GPH anomalies marked by high-pressure systems over mid-latitudes act as a thermodynamic barrier, suppressing the northward incursion of tropical moisture. This configuration not only amplifies aridity over northern regions but also reduces snowfall potential,

as the cold, moisture-starved conditions limit cloud formation and precipitation efficiency. The resultant snow cover decline in CA and the TP is thus intrinsically tied to this circulation-driven moisture deficit, compounded by radiative cooling under clear skies, which enhances sublimation of existing snowpack.

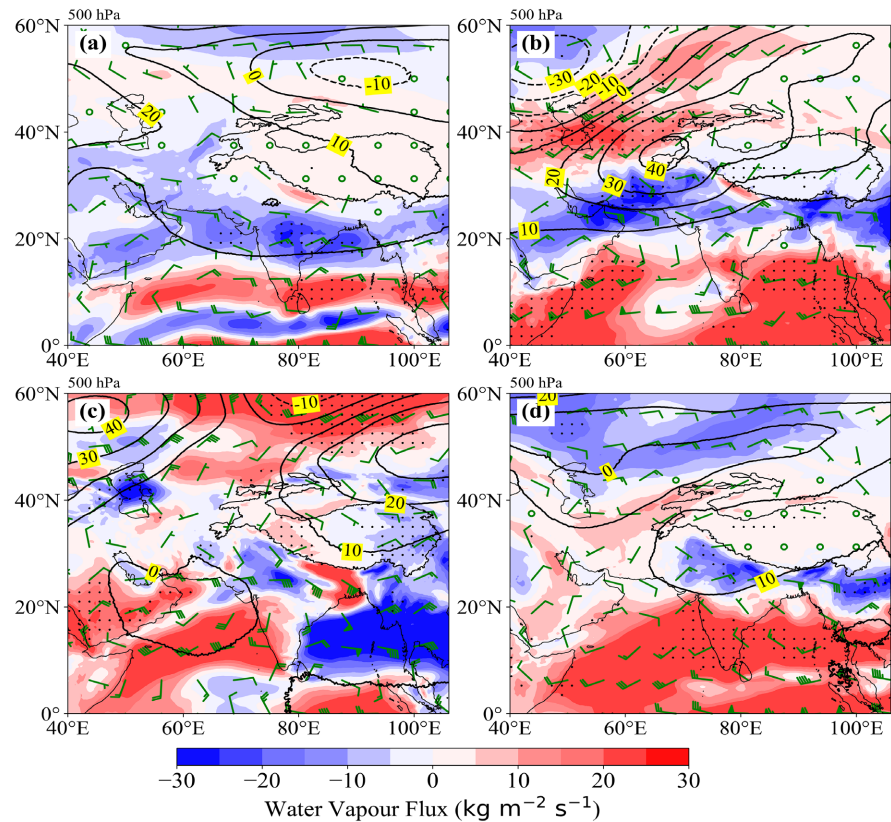


Figure 11. Seasonal distributional pattern of atmospheric circulation and moisture anomalies at 500 hPa. (a) DJF, (b) MAM, (c) JJA, and (d) SON. Shading indicates water vapor flux ($\text{kg m}^{-2} \text{s}^{-1}$) differences with stippling regions with significant regions ($p < 0.05$). Black contours show the geopotential height (GPH, m) anomalies, labelled yellow. Wind vector (U and V) anomalies are shown in green bars (max15 m/s), and green circles highlight areas with wind speeds below 5 m/s.

Transitioning into spring (**Figure 11(b)**), the emergence of a dipole pattern characterized by persistent drying over CA and enhanced moisture flux over the southeastern Himalayas highlights the seasonal reorganization of atmospheric dynamics. The strengthening of the Eurasian westerly jet stream, evidenced by intensified wind barbs, facilitates anomalous moisture transport from the Arabian Sea toward northern latitudes. However, this moisture is preferentially funneled into orographic uplift zones along the Himalayas, leaving CA under subsiding air masses associated with mid-level ridging. The altered GPH contours further indicate a weakening of the Siberian High and a northward shift of the subtropical ridge, which redistributes moisture toward convective hotspots over the Indian subcontinent. For snow cover, this season marks a critical transition: while enhanced westerly-derived moisture may temporarily augment snowfall in high-al-

titude regions, rising temperatures and increased insolation accelerate snowmelt, particularly in areas where adiabatic warming from subsiding winds dominates. The net effect is a reduction in spring snowpack, exacerbated by earlier melt onset linked to circulation-driven thermal advection.

The dominance of the South Asian monsoon introduces a stark contrast in moisture regimes (**Figure 11(c)**) during summer. Widespread positive water vapor flux anomalies over Indochina and East Asia (EA) reflect the influx of oceanic moisture via robust southerly monsoon winds, while CA remains entrenched in arid conditions. The monsoon's meridional circulation strengthens moisture convergence over land, yet the concurrent weakening of monsoon intensity over the Indian subcontinent evident in diminished wind vector magnitudes underscores regional heterogeneity in precipitation delivery. For snow-covered regions, this season presents a dual influence: enhanced monsoon rains at lower elevations reduce snow accumulation, while persistent high-pressure systems over CA maintain clear skies and elevated temperatures, further depleting residual snow reserves. Moreover, the interaction between monsoon-derived humidity and mid-latitude troughs can trigger episodic snowfall in high-altitude zones, though such events are insufficient to offset the overarching trend of reduced snow duration and extent.

The atmospheric circulation transitions to a zonally symmetric pattern, marked by drying across northern latitudes and moisture convergence in southern regions during autumn (**Figure 11(d)**). The westward displacement of the East Asia (EA) jet stream, coupled with a weakened mid-latitude westerly belt and a reinforced subtropical ridge, redirects moisture pathways toward the Indian Ocean and Maritime Continent (IOMC). This reconfiguration diminishes the advection of cold air into northern regions while enhancing warm, dry subsidence over CA and the TP. The resultant snow cover changes are twofold: delayed autumn snowfall in northern areas due to prolonged warmth and moisture scarcity, contrasted with sporadic early-season snow events in southern highlands where residual moisture convergence persists. Critically, the weakening of cyclonic activity over Siberia reduces the frequency of snow-bearing frontal systems, further diminishing snow initialization across continental interiors.

The interplay between these seasonal circulation anomalies and snow cover dynamics is fundamentally rooted in the thermodynamics and kinematics of general circulation. High-pressure anomalies in winter and autumn suppress cloud cover and precipitation, while favoring radiative cooling and sublimation processes that deplete snowpack despite cold temperatures. Conversely, spring and summer circulation shifts modulate snowmelt through thermal advection and moisture redistribution, with jet stream variability acting as a pivotal driver of both moisture delivery and temperature regimes. Additionally, the intensification of meridional circulation patterns under a warming climate amplifies these effects, as evidenced by the increasing frequency of blocking highs and attenuated monsoonal flows. These mechanisms collectively underscore the sensitivity of snow cover to atmos-

pheric circulation, with implications for albedo feedbacks, freshwater resources, and regional climate resilience.

5. Discussions

The observed decline in snow cover across the WTP aligns with broader climatic trends on the TP, where rising temperatures have been identified as the dominant driver of snow loss. The most pronounced reductions in spring and summer (-0.16% and $-0.93\% 10a^{-1}$) reflect the heightened sensitivity of seasonal snowpack to warming, particularly at high altitudes. These trends, validated by NSIDC and ERA5 datasets, mirror findings from Huang *et al.* [36] and Yao *et al.* [42], who similarly linked temperature increases to snow cover retreat on the Tibetan Plateau. The statistical significance of these trends underscores the accelerating impact of global warming on regional cryospheric systems. Beyond temperature, snow cover variability is modulated by large-scale climate indices. Positive phases of the NAO, IOD, and ENSO correlate with reduced snow accumulation, mediated through shifts in atmospheric circulation. For instance, the NAO and IOBW amplify dry, cold air advection, suppressing precipitation and SCF, while El Niño-induced warming in the eastern Pacific enhances subsidence over the WTP, limiting SD and moisture availability. These dynamics highlight the dual influence of Atlantic and Pacific climate systems on regional snow dynamics, consistent with studies by Jiang *et al.* [43] and Wang *et al.* [44]. The weaker but coherent correlation between SD and the Niño3 index further emphasizes the role of remote oceanic forcing in modulating snow accumulation. The convergence of warming-driven snow loss and climate index impacts exacerbates the vulnerability of the WTP's hydrology. Snowmelt from the plateau sustains major river systems in South and East Asia, and declining snow cover threatens water security for downstream populations. While precipitation changes remain uncertain in climate projections, the dominant temperature signal suggests irreversible snow cover reductions under continued warming. This necessitates improved climate models to resolve regional feedback mechanisms, particularly the interplay between atmospheric-oceanic patterns and local topography.

6. Conclusion

This study identifies rising temperatures as the primary driver of declining snow cover over the WTP, with spring and summer losses posing critical risks to regional water resources. Large-scale climate indices, including the NAO, IOD, and ENSO, further modulate snow dynamics by altering temperature and precipitation patterns, underscoring the plateau's sensitivity to global climatic processes. The findings highlight two urgent priorities. First, the WTP's hydrological systems require adaptive management strategies to address diminishing snowmelt, a key water source for Asia's major river basins. Second, advancements in climate modeling are essential to better predict interactions between warming, atmospheric circulation, and snow cover. Future research must prioritize sustained

monitoring of snow metrics and mechanistic studies to disentangle regional vs. global drivers of change. Such efforts will enhance the accuracy of hydrological forecasts and inform policies to mitigate climate risks. Understanding the intricate connections between snow metrics and climate indices is crucial for guiding informed policy decisions and securing the long-term sustainability of water resources in the South and East Asia.

Acknowledgements

This work was supported by the National Natural Science Foundation of China (Grant No. 42175064 and 41471034) and the Natural Science Foundation of Gansu Province of China (Grant No. 20JR10RA654). We extend our gratitude to the Supercomputing Centre of Lanzhou University for providing the computational resources necessary for this study.

Data Availability Statement

The weekly Northern Hemisphere snow cover dataset (NSIDC) is available at <https://nsidc.org/data/nsidc-0046/versions/4>. The daily snow depth dataset can be accessed at <https://data.tpdc.ac.cn/en/data/9764584a-f2df-455b-96ef-8e8968a230fa>. The monthly means temperature and precipitation data of ERA5 reanalysis dataset is freely available through the Copernicus Climate Change Service (C3S) Climate Data Store at <https://cds.climate.copernicus.eu/datasets/reanalysis-era5-land-monthly-means> and the ECMWF archive at <https://www.ecmwf.int/en/forecasts/datasets/archive-datasets>. Climate index datasets used in this study can be accessed at <http://cmdp.ncc-cma.net/cn/monitoring.htm>.

Conflicts of Interest

The authors declare no conflicts of interest regarding the publication of this paper.

References

- [1] Barnett, T.P., Dümenil, L., Schlese, U., Roeckner, E. and Latif, M. (1989) The Effect of Eurasian Snow Cover on Regional and Global Climate Variations. *Journal of the Atmospheric Sciences*, **46**, 661-686. [https://doi.org/10.1175/1520-0469\(1989\)046<0661:teoesc>2.0.co;2](https://doi.org/10.1175/1520-0469(1989)046<0661:teoesc>2.0.co;2)
- [2] Yasunari, T., Kitoh, A. and Tokioka, T. (1991) Local and Remote Responses to Excessive Snow Mass over Eurasia Appearing in the Northern Spring and Summer Climate. *Journal of the Meteorological Society of Japan. Ser. II*, **69**, 473-487. https://doi.org/10.2151/jmsj1965.69.4_473
- [3] Lutz, A.F., Immerzeel, W.W., Shrestha, A.B. and Bierkens, M.F.P. (2014) Consistent Increase in High Asia's Runoff Due to Increasing Glacier Melt and Precipitation. *Nature Climate Change*, **4**, 587-592. <https://doi.org/10.1038/nclimate2237>
- [4] Wang, C., Yang, K., Li, Y., Wu, D. and Bo, Y. (2017) Impacts of Spatiotemporal Anomalies of Tibetan Plateau Snow Cover on Summer Precipitation in Eastern China. *Journal of Climate*, **30**, 885-903. <https://doi.org/10.1175/jcli-d-16-0041.1>

- [5] Chu, D., Liu, L. and Wang, Z. (2023) Snow Cover on the Tibetan Plateau and Topographic Controls. *Remote Sensing*, **15**, Article 4044. <https://doi.org/10.3390/rs15164044>
- [6] Deng, H. and Ji, Z. (2023) Warming and Wetting Will Continue over the Tibetan Plateau in the Shared Socioeconomic Pathways. *PLOS ONE*, **18**, e0289589. <https://doi.org/10.1371/journal.pone.0289589>
- [7] Fallah, B., Rostami, M., Didovets, I. and Dong, Z. (2024) High-Resolution CMIP6 Analysis Highlights Emerging Climate Challenges in Alpine and Tibetan Tundra Zones. *Meteorological Applications*, **31**, e70001. <https://doi.org/10.1002/met.70001>
- [8] Li, Y., Wang, C., Tang, Q., Yao, S., Sun, B., Peng, H., et al. (2024) Unraveling the Discrepancies between Eulerian and Lagrangian Moisture Tracking Models in Monsoon- and Westerly-Dominated Basins of the Tibetan Plateau. *Atmospheric Chemistry and Physics*, **24**, 10741-10758. <https://doi.org/10.5194/acp-24-10741-2024>
- [9] Wang, B., Zhao, L. and Li, Y. (2023) Temporal and Spatial Variation Characteristics of Snow Cover Area in the Pamirs from 2010 to 2020. *Open Journal of Applied Sciences*, **13**, 109-119. <https://doi.org/10.4236/ojapps.2023.131010>
- [10] Ma, Q., Keyimu, M., Li, X., Wu, S., Zeng, F. and Lin, L. (2023) Climate and Elevation Control Snow Depth and Snow Phenology on the Tibetan Plateau. *Journal of Hydrology*, **617**, Article 128938. <https://doi.org/10.1016/j.jhydrol.2022.128938>
- [11] Bormann, K.J., Brown, R.D., Derksen, C. and Painter, T.H. (2018) Estimating Snow-Cover Trends from Space. *Nature Climate Change*, **8**, 924-928. <https://doi.org/10.1038/s41558-018-0318-3>
- [12] IPCC (2021) Future Global Climate: Scenario-Based Projections and Near-Term Information. In: Intergovernmental Panel on Climate Change (IPCC) Ed., *Climate Change 2021: The Physical Science Basis. Contribution of Working Group I to the Sixth Assessment Report of the Intergovernmental Panel on Climate Change*, Cambridge University Press, 553-672. <https://doi.org/10.1017/9781009157896.006>
- [13] Huang, J., Zhou, X., Wu, G., Xu, X., Zhao, Q., Liu, Y., et al. (2023) Global Climate Impacts of Land-Surface and Atmospheric Processes over the Tibetan Plateau. *Reviews of Geophysics*, **61**, RG000771. <https://doi.org/10.1029/2022rg000771>
- [14] Li, L., Shen, M., Hou, Y., Xu, C., Lutz, A.F., Chen, J., et al. (2019) Twenty-First-Century Glacio-Hydrological Changes in the Himalayan Headwater Beas River Basin. *Hydrology and Earth System Sciences*, **23**, 1483-1503. <https://doi.org/10.5194/hess-23-1483-2019>
- [15] Rikiishi, K. and Nakasato, H. (2006) Height Dependence of the Tendency for Reduction in Seasonal Snow Cover in the Himalaya and the Tibetan Plateau Region, 1966-2001. *Annals of Glaciology*, **43**, 369-377. <https://doi.org/10.3189/172756406781811989>
- [16] Viste, E. and Sorteberg, A. (2015) Snowfall in the Himalayas: An Uncertain Future from a Little-Known Past. *The Cryosphere*, **9**, 1147-1167. <https://doi.org/10.5194/tc-9-1147-2015>
- [17] Orsolini, Y., Wegmann, M., Dutra, E., Liu, B., Balsamo, G., Yang, K., et al. (2019) Evaluation of Snow Depth and Snow Cover over the Tibetan Plateau in Global Reanalyses Using in Situ and Satellite Remote Sensing Observations. *The Cryosphere*, **13**, 2221-2239. <https://doi.org/10.5194/tc-13-2221-2019>
- [18] Khadka, N., Chen, X., Sharma, S. and Shrestha, B. (2023) Climate Change and Its Impacts on Glaciers and Glacial Lakes in Nepal Himalayas. *Regional Environmental Change*, **23**, Article No. 143. <https://doi.org/10.1007/s10113-023-02142-y>
- [19] Panicker, D.V., Vachharajani, B.H. and Srivastava, R. (2024) Spatiotemporal Varia-

- bility of Snow Parameters over Himalayan-Tibetan Region Utilizing ERA-5 Data. *Journal of the Indian Society of Remote Sensing*, **52**, 957-972. <https://doi.org/10.1007/s12524-024-01830-4>
- [20] Forsythe, N., Fowler, H.J., Li, X., Blenkinsop, S. and Pritchard, D. (2017) Karakoram Temperature and Glacial Melt Driven by Regional Atmospheric Circulation Variability. *Nature Climate Change*, **7**, 664-670. <https://doi.org/10.1038/nclimate3361>
- [21] Farinotti, D., Immerzeel, W.W., de Kok, R.J., Quincey, D.J. and Dehecq, A. (2020) Manifestations and Mechanisms of the Karakoram Glacier Anomaly. *Nature Geoscience*, **13**, 8-16. <https://doi.org/10.1038/s41561-019-0513-5>
- [22] Curio, J., Maussion, F. and Scherer, D. (2015) A 12-Year High-Resolution Climatology of Atmospheric Water Transport over the Tibetan Plateau. *Earth System Dynamics*, **6**, 109-124. <https://doi.org/10.5194/esd-6-109-2015>
- [23] Zhao, R., Chen, B., Zhang, W., Yang, S. and Xu, X. (2024) Formation Mechanisms of Persistent Extreme Precipitation Events over the Eastern Periphery of the Tibetan Plateau: Synoptic Conditions, Moisture Transport and the Effect of Steep Terrain. *Atmospheric Research*, **304**, Article 107341. <https://doi.org/10.1016/j.atmosres.2024.107341>
- [24] Tang, Z., Wang, J., Li, H. and Yan, L. (2013) Spatiotemporal Changes of Snow Cover over the Tibetan Plateau Based on Cloud-Removed Moderate Resolution Imaging Spectroradiometer Fractional Snow Cover Product from 2001 to 2011. *Journal of Applied Remote Sensing*, **7**, Article 073582. <https://doi.org/10.1117/1.jrs.7.073582>
- [25] Zhang, P. and Duan, A. (2021) Dipole Mode of the Precipitation Anomaly over the Tibetan Plateau in Mid-Autumn Associated with Tropical Pacific-Indian Ocean Sea Surface Temperature Anomaly: Role of Convection over the Northern Maritime Continent. *Journal of Geophysical Research: Atmospheres*, **126**, JD034675. <https://doi.org/10.1029/2021jd034675>
- [26] Gao, Y., Dong, H., Dai, Y., Mou, N. and Wei, W. (2023) Contrasting Changes of Snow Cover between Different Regions of the Tibetan Plateau during the Latest 21 Years. *Frontiers in Earth Science*, **10**, Article 1075988. <https://doi.org/10.3389/feart.2022.1075988>
- [27] Peings, Y. and Douville, H. (2009) Influence of the Eurasian Snow Cover on the Indian Summer Monsoon Variability in Observed Climatologies and CMIP3 Simulations. *Climate Dynamics*, **34**, 643-660. <https://doi.org/10.1007/s00382-009-0565-0>
- [28] Cherchi, A. and Navarra, A. (2012) Influence of ENSO and of the Indian Ocean Dipole on the Indian Summer Monsoon Variability. *Climate Dynamics*, **41**, 81-103. <https://doi.org/10.1007/s00382-012-1602-y>
- [29] Halder, S. and Dirmeyer, P.A. (2017) Relation of Eurasian Snow Cover and Indian Summer Monsoon Rainfall: Importance of the Delayed Hydrological Effect. *Journal of Climate*, **30**, 1273-1289. <https://doi.org/10.1175/jcli-d-16-0033.1>
- [30] Rupp, P. and Haynes, P. (2021) Zonal Scale and Temporal Variability of the Asian Monsoon Anticyclone in an Idealised Numerical Model. *Weather and Climate Dynamics*, **2**, 413-431. <https://doi.org/10.5194/wcd-2-413-2021>
- [31] Mehmood, S., Ashfaq, M., Kapnick, S., Gosh, S., Abid, M.A., Kucharski, F., et al. (2022) Dominant Controls of Cold-Season Precipitation Variability over the High Mountains of Asia. *NPJ Climate and Atmospheric Science*, **5**, Article No. 65. <https://doi.org/10.1038/s41612-022-00282-2>
- [32] Ibebuchi, C.C. (2022) Circulation Patterns Linked to the Positive Sub-Tropical Indian Ocean Dipole. *Advances in Atmospheric Sciences*, **40**, 110-128. <https://doi.org/10.1007/s00376-022-2017-2>

- [33] Kang, S., Xu, Y., You, Q., Flügel, W., Pepin, N. and Yao, T. (2010) Review of Climate and Cryospheric Change in the Tibetan Plateau. *Environmental Research Letters*, **5**, Article 015101. <https://doi.org/10.1088/1748-9326/5/1/015101>
- [34] Yao, T., Thompson, L., Yang, W., Yu, W., Gao, Y., Guo, X., et al. (2012) Different Glacier Status with Atmospheric Circulations in Tibetan Plateau and Surroundings. *Nature Climate Change*, **2**, 663-667. <https://doi.org/10.1038/nclimate1580>
- [35] Immerzeel, W.W., van Beek, L.P.H. and Bierkens, M.F.P. (2010) Climate Change Will Affect the Asian Water Towers. *Science*, **328**, 1382-1385. <https://doi.org/10.1126/science.1183188>
- [36] Huang, X., Deng, J., Wang, W., Feng, Q. and Liang, T. (2017) Impact of Climate and Elevation on Snow Cover Using Integrated Remote Sensing Snow Products in Tibetan Plateau. *Remote Sensing of Environment*, **190**, 274-288. <https://doi.org/10.1016/j.rse.2016.12.028>
- [37] Brodzik, M. J. & Armstrong, R. (2013) Northern Hemisphere EASE-Grid 2.0 Weekly Snow Cover and Sea Ice Extent. (NSIDC-0046, Version 4). NASA National Snow and Ice Data Center Distributed Active Archive Center. <https://doi.org/10.5067/P7O0HGJLYUQU>
- [38] Dai, L., Che, T. and Ding, Y. (2015) Inter-Calibrating SMMR, SSM/I and SSMI/S Data to Improve the Consistency of Snow-Depth Products in China. *Remote Sensing*, **7**, 7212-7230. <https://doi.org/10.3390/rs70607212>
- [39] Lavers, D.A., Simmons, A., Vamborg, F. and Rodwell, M.J. (2022) An Evaluation of ERA5 Precipitation for Climate Monitoring. *Quarterly Journal of the Royal Meteorological Society*, **148**, 3152-3165. <https://doi.org/10.1002/qj.4351>
- [40] Zhou, B., Xu, Y., Wu, J., Dong, S. and Shi, Y. (2015) Changes in Temperature and Precipitation Extreme Indices over China: Analysis of a High-Resolution Grid Dataset. *International Journal of Climatology*, **36**, 1051-1066. <https://doi.org/10.1002/joc.4400>
- [41] Che, T., Li, X., Jin, R., Armstrong, R. and Zhang, T. (2008) Snow Depth Derived from Passive Microwave Remote-Sensing Data in China. *Annals of Glaciology*, **49**, 145-154. <https://doi.org/10.3189/172756408787814690>
- [42] Yao, T., Xue, Y., Chen, D., Chen, F., Thompson, L., Cui, P., et al. (2019) Recent Third Pole's Rapid Warming Accompanies Cryospheric Melt and Water Cycle Intensification and Interactions between Monsoon and Environment: Multidisciplinary Approach with Observations, Modeling, and Analysis. *Bulletin of the American Meteorological Society*, **100**, 423-444. <https://doi.org/10.1175/bams-d-17-0057.1>
- [43] Jiang, X., Zhang, T., Tam, C., Chen, J., Lau, N., Yang, S., et al. (2019) Impacts of ENSO and IOD on Snow Depth over the Tibetan Plateau: Roles of Convections over the Western North Pacific and Indian Ocean. *Journal of Geophysical Research: Atmospheres*, **124**, 11961-11975. <https://doi.org/10.1029/2019jd031384>
- [44] Wang, H., Sun, J., Fu, S. and Zhang, Y. (2021) Typical Circulation Patterns and Associated Mechanisms for Persistent Heavy Rainfall Events over Yangtze-Huaihe River Valley during 1981-2020. *Advances in Atmospheric Sciences*, **38**, 2167-2182. <https://doi.org/10.1007/s00376-021-1194-8>

Abbreviations

Abbreviation	Full Terminology
TP	Tibetan Plateau
WTP	Western Tibetan Plateau
SCF	Snow Cover Fraction
SD	Snow Depth
sde.	Standard Deviation
NSIDC	National Snow and Ice Data Center
NTPDC	National Tibetan Plateau Data Center
NCC	National Climate Center of China
LR	Linear Regression
RMSE	Room Mean Square Error
SST	Sea surface temperature
ENSO	El Niño Southern Oscillation
IOBW	Indian Ocean Basin Wide
TIOD	Tropical Indian Ocean Dipole
SIOD	Subtropical Indian Ocean Dipole
NAO	North Atlantic Oscillation
IOSST	Indian Ocean Sea Surface Temperature
GPH	Geopotential Height
T	Temperature
Pre.	Precipitation
Q	Specific Humidity
W	U and V Wind Components